

Exploring the Application of the Multiphase Eulerian Model for Nanofluids in Microchannel at Elevated Volume Fractions

Muhammad M. Generous¹, Anas Alazzam², Eiyad Abu-Nada²

¹Khalifa University
Abu Dhabi, United Arab Emirates
100061031@ku.ac.ae; anas.alazzam@ku.ac.ae

²Khalifa University
Abu Dhabi, United Arab Emirates
eiyad.abunada@ku.ac.ae

Abstract - This study focuses on modeling of Al₂O₃-water nanofluids energy transport in a microchannel using multiphase Eulerian model. The study of the Knudsen number showed that continuum can be assumed above volume fraction 2.5%. Therefore, conservation equations can be used to solve both phases separately. In addition to conservation equation, an effort has been made to model fluid-solid interaction, solid-solid interaction, and interphase heat transfer. Various phenomenon such as shear viscosity, bulk viscosity, granular temperature, wall lubrication forces, virtual mass forces, lift, and drag forces are modelled. Moreover, interphase heat transfer is modelled. Finally, this comprehensive model is used to study heat transfer enhancement of Al₂O₃-water nanofluids with volume fraction of 3%, 4%, 5%, and 6%. It is found that the heat transfer increases with increase in volume fraction of the solid phase in the range considered in this study. The comparison of the average heat transfer coefficient of water with Al₂O₃-water nanofluids showed that heat transfer coefficient enhancement of 9.35%, 14.48%, 19.1%, and 23.5% at volume fraction of 3%, 4%, 5%, and 6%, respectively.

Keywords: multiphase Eulerian model; interphase momentum exchange; interphase heat exchange, fluid-solid interaction, solid-solid interaction

1. Introduction

Nanofluids consist of nanoparticles dispersed within a base fluid, manifesting intricate and distinctive multiphase characteristics. To elucidate the behavior of nanofluids, multiple multiphase models have been devised, with select examples presented below. The selection of an appropriate model hinges on the particular application and the degree of precision needed to accurately characterize nanofluid behavior [1].

The initial category of models falls within the ambit of two-phase models. These models conceptualize nanofluids as biphasic amalgamations comprising nanoparticles and the foundational fluid. This biphasic amalgamation is conventionally assumed to maintain local thermal equilibrium, and the movement of nanoparticles is dictated by principles of momentum, energy, and mass conservation [2]. These models can be subcategorized into single-phase models, where nanoparticles are presumed to be homogeneously dispersed within the fluid, or two-phase models, wherein distinct dispersed and continuous phases are considered [3].

The second classification encompasses multiphase flow models. These models are designed to accommodate the coexistence of diverse phases within the nanofluid, encompassing interaction between phases, and addressing the intricate interplay of mass, momentum, and energy transfer between these phases. Multiphase flow models can be further subdivided into two main categories: Eulerian-Eulerian models, where each phase is considered as an independent continuum, and Eulerian-Lagrangian models, wherein the nanoparticles are meticulously traced as Lagrangian particles within the fluid medium [4].

The final modeling approach for nanofluids is the hybrid approach. These models amalgamate elements from two or more of the aforementioned models to encapsulate the distinctive characteristics of nanofluids. As an illustration, a hybrid model that combines features from both two-phase and three-phase models can be employed to investigate phenomena such as nanoparticle deposition and suspension behavior within a nanofluid system [5].

In summary, Eulerian multiphase modeling stands as a robust instrument for forecasting the performance of nanofluids across a spectrum of applications, such as electronic cooling [6]. Nonetheless, it remains imperative to rigorously corroborate model outcomes through empirical data and to judiciously acknowledge the inherent constraints and presumptions within the model.

Eulerian multiphase modeling is a widely adopted methodology employed for simulating the dynamics of nanofluids. Within this framework, the nanofluid is conceptualized as a two-phase system, comprising a continuous phase (representing the base fluid) and a dispersed phase (comprising the nanoparticles) [7].

The fundamental equations that govern Eulerian multiphase modeling of nanofluids encompass the continuity equation, momentum equation, and energy equation for each individual phase. Additionally, an extra transport equation is incorporated to account for the volume fraction of the dispersed phase. To forecast the nanofluid's behavior, these transport equations are systematically solved employing numerical techniques like the finite volume method or the finite element method [8].

An inherent strength of Eulerian multiphase modeling lies in its ability to precisely capture the dispersion and concentration of nanoparticles within the base fluid, facilitating precise forecasts of heat transfer performance [8]. Furthermore, this model possesses the capacity to factor in the influence of nanoparticle characteristics, including size, morphology, and surface chemistry, on the transport and deposition of nanoparticles within the fluid flow. Nonetheless, it's noteworthy that Eulerian multiphase modeling can demand substantial computational resources due to its computational intensity. Additionally, it necessitates accurate input parameters, such as the thermophysical properties of both nanoparticles and the base fluid, which can pose challenges when attempting experimental measurement.

In the current investigation, the chosen modeling approach is Eulerian, specifically involving the separate solution of each phase, as outlined in reference [8]. However, it's imperative to establish a continuum for each phase in order to apply the principles of mass conservation, energy conservation, and momentum conservation effectively. This necessitates an examination of the Knudsen number for the nanofluids under study, ensuring that each phase can indeed be regarded as a continuum. Generally, a Knudsen number value below 0.01 is considered acceptable for characterizing the phase under consideration as a continuum, as discussed in reference [9]. The current study demonstrated that for Al_2O_3 nanoparticles in water as base fluid, the Knudsen number is less than 0.01 when the volume fraction of solid phase is 2.5%, as shown in Fig. 1.

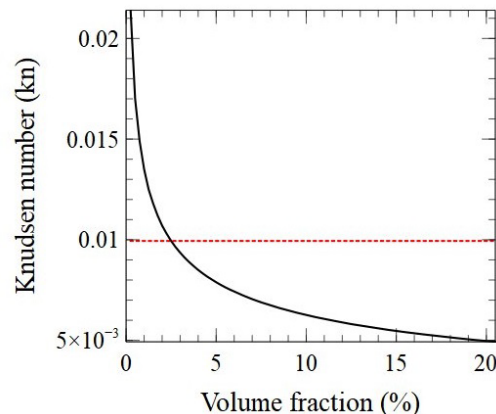


Fig. 1. Knudsen number against volume fraction of solid particles.

2. System Description

In the present study, a circular microchannel featuring a constant heat flux configuration is employed. The microchannel is characterized by a hydraulic diameter of 210 micrometers and a length of 46.62 millimeters. The heat transfer behavior within this circular microchannel, subject to a constant heat flux, is contingent upon several influential

parameters. These parameters encompass the channel's diameter, fluid properties, heat flux magnitude, and flow rate. It is noteworthy that circular microchannels, in general, offer a superior surface area-to-volume ratio compared to their rectangular counterparts, resulting in heightened heat transfer efficiency. Circular microchannels sustaining a constant heat flux are of paramount significance in a spectrum of microscale heat transfer applications, where compact and efficient efficient cooling or heating is imperative. The design and optimization of such microchannels necessitate meticulous consideration of flow conditions, thermal characteristics, and geometrical attributes to achieve the desired heat transfer efficacy.

In this study, aluminum oxide nanoparticles are modeled using the Eulerian multiphase model, with water serving as the base fluid. These spherical particles exhibit a diameter of 150 nanometers. The inlet temperature is fixed at 30 degrees Celsius, while the pressure outlet boundary condition is defined at the channel's outlet, ensuring a constant gauge pressure of zero. Additionally, a gravitational force is applied in the negative y-direction.

The microchannel geometry adheres to a circular shape cross-section, with an inner diameter of 210 μm and a length of 46.62 mm. A consistent heat flux of 100,000 W/m^2 is applied to the channel walls, while the inlet volume fraction varies within the range of 3% to 6%. A polyhedral mesh comprising 122,188 elements is employed. The geometry and mesh type are depicted in Fig. 2, and the pertinent material properties of alumina and water used in this research are detailed in Table 1.

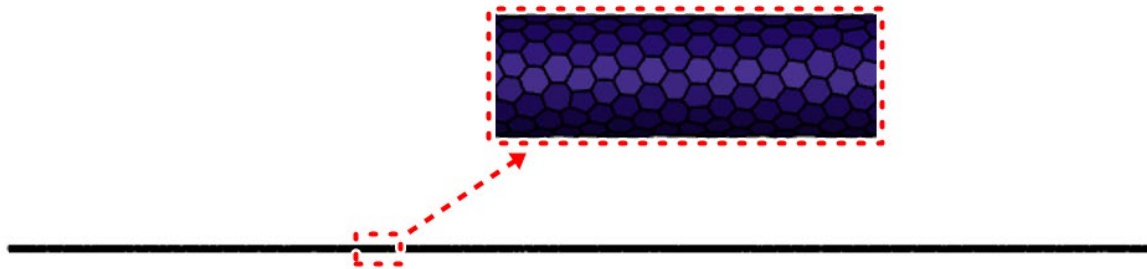


Fig. 2. Geometry and mesh used in the present model.

Table 1. Properties of the phases used in this study.

Phase	C_p (J/kg.K)	K (W/m.K)	ρ (kg/m ³)
Water	4182	0.6	998.2
Al_2O_3	900	27	3900

3. Mathematical Modeling

The Eulerian model stands as a prevalent method within computational fluid dynamics (CFD), employed to simulate multiphase flows involving the coexistence of two or more phases within the flow domain. In this approach, it is postulated that the phases exhibit a uniform distribution and are represented as interpenetrating continua. The governing equations are independently solved for each of these phases. Governing equation for multiphase Eulerian model is mainly comprised of mass conservation, momentum conservation, and energy conservation. Steady-state continuity is solved for each phase, as [10]:

$$\frac{\partial}{\partial t}(\phi_j \rho_j) + \nabla \cdot (\phi_j \rho_j \mathbf{V}_j) = S_j \quad (1)$$

Where ϕ_j is volume fraction, ρ_j is density (in kg/m^3) and S_j is source term which is zero in the current study. Momentum conservation is modelled using momentum equation for each phase separately in addition to the interphases interactions such interphases force transfer, lift force, wall lubrication force, virtual mass force, and turbulent dispersion force. The momentum conservation is modelled as [8]:

$$\frac{\partial}{\partial t} (\phi_j \rho_j \mathbf{V}_j) + \nabla \cdot (\phi_j \rho_j \mathbf{V}_j \mathbf{V}_j) = -\phi_j \nabla P + \nabla \cdot \bar{\boldsymbol{\tau}}_j + \phi_j \rho_j \mathbf{g} + \sum_{i=1}^n (\mathbf{R}_{ij}) + (\vec{F}_{lift,j} + \vec{F}_{wl,j} + \vec{F}_{vm,j} + \vec{F}_{td,j}) \quad (2)$$

where ρ (in kg/m³) is density, \mathbf{V} (in m/s) is velocity vector, P (in Pa) is pressure, $\bar{\boldsymbol{\tau}}_j$ is stress strain tensor, \mathbf{R}_{ij} is interaction forces, $\vec{F}_{lift,j}$ is lift force, $\vec{F}_{wl,j}$ is wall lubrication force, $\vec{F}_{vm,j}$ is virtual mass force, and $\vec{F}_{td,j}$ is turbulent force which is zero as flow limited to low Reynolds number. Interphases forces transfer can be calculated as [8]:

$$\sum_{i=1}^n \mathbf{R}_{ij} = \sum_{i=1}^n \mathbf{K}_{ij} (V_i - V_j) \quad (3)$$

The solids stress tensor contains shear and bulk viscosities arising from particle momentum exchange due to translation and collision. A frictional component of viscosity can also be included to account for the viscous-plastic transition that occurs when particles of a solid phase reach the maximum solid volume fraction. Shear viscosity is comprised of collision parts, kinematics part, and frictional component.

$$\mu_s = \mu_{col} + \mu_{kin} + \mu_{fr} \quad (4)$$

The granular temperature of solid phase particles is proportional to kinetic energy of particles which comes from the following transport equation:

$$\frac{\partial}{\partial t} (\phi_s \rho_s \boldsymbol{\theta}_s) + \nabla \cdot (\phi_s \rho_s \mathbf{V}_s \boldsymbol{\theta}_s) = (-P_s I + \bar{\boldsymbol{\tau}}_s) : \nabla \mathbf{V}_s + \nabla \cdot (D \nabla \boldsymbol{\theta}_s) - Y_s + \beta_{ls} \quad (5)$$

$(-P_s I + \bar{\boldsymbol{\tau}}_s) : \nabla \mathbf{V}_s$ is energy generation by solid stress, $D \nabla \boldsymbol{\theta}_s$ is diffusion of energy, Y_s is collision dissipation of energy, and β_{ls} is transfer of kinetic energy due to random fluctuations. Where α is specularity coefficient between particle and walls. V_{slip} is slip velocity. Energy conservation is modelled using energy equation in addition to modeling interphase heat exchange between various phases, as [8]:

$$\frac{\partial}{\partial t} (\phi_q \rho_q h_q) + \nabla \cdot (\phi_q \rho_q \mathbf{V}_q h_q) = -\phi_q \nabla P + \bar{\boldsymbol{\tau}}_q : \nabla \cdot \mathbf{u}_q + S_q + \sum_{p=1}^n (Q_{pq}) \quad (6)$$

Where h_q is specific enthalpy, q_q is applied heat flux the walls, S_q is source term which is zero in this study, and Q_{pq} is interphases heat exchange.

4. Results and Discussion

4.1. Mesh Independence Study

In the context of this study, a meticulous examination of mesh independence was conducted. The initial mesh consisted of 50,149 polyhedral elements. This mesh was systematically refined, leading to an incremental increase in the number of elements. A critical observation emerged from this mesh independence analysis: beyond a certain threshold, specifically when the mesh reached 100,000 cells, no substantial improvement in simulation results was discernible.

4.2. Model Validation

This validation process involves a rigorous comparison between the model's predictions and experimental data provided by Vafaei et al. [11], specifically considering two distinct volume concentrations of 2.76% and 6%. The primary objective of this validation exercise is to assess the model's capacity to predict the Nusselt number as a function of dimensionless axial distance. A remarkable level of agreement is observed between the model's predictions and the experimental data. Specifically, for the case with a 2.76% volume concentration, the deviation from the experimental data is merely 2.4%. Similarly, for the 6% volume concentration case, the model exhibits an exceptionally close fit with the experimental data, with a deviation of only 0.34%.

The close alignment between the model's predictions and experimental observations, as visually represented in Fig. 3, underscores the model's reliability in capturing the underlying physical phenomena. This high level of agreement instills confidence in the model's predictive capabilities and affirms its suitability for further application and analysis in the context of electroosmotic desalination processes.

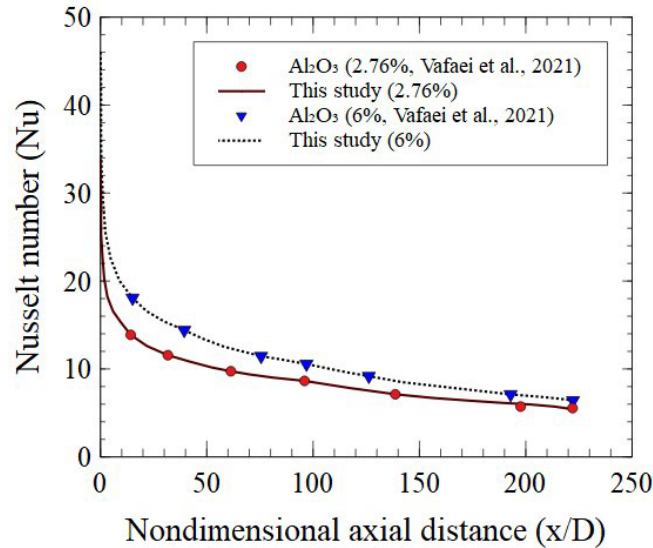


Fig. 3. Model validation against the local Nusselt number data provided by Vafaei et al. [11].

4.3. Results

The validated model serves as a powerful tool for an in-depth exploration of several critical aspects, including heat transfer enhancement, pressure drop, and the influence of gravity on the sedimentation of nanoparticles within the base fluid. The role of gravity emerges as a particularly significant factor with profound implications for both heat transfer and particle behavior within the fluid medium, which, in this case, is water.

The parabolic velocity profile is a consequence of a fundamental principle in fluid dynamics known as the "no-slip condition" at the boundary or wall. According to this principle, at a solid boundary, such as the wall in this case, the fluid velocity is effectively zero due to the frictional interaction between the fluid and the stationary surface. As one moves away from the wall into the fluid, the velocity gradually increases until it reaches its maximum value at the center of the duct. This results in the classic parabolic velocity distribution, a well-documented and essential characteristic of fluid flow near solid boundaries.

Understanding this parabolic velocity profile is crucial in various engineering and scientific applications, as it provides insights into the behavior of fluids in confined spaces and contributes to the prediction of flow patterns, pressure drops, and heat transfer rates within such systems. Therefore, Fig. 4 not only visually captures this fundamental fluid dynamic phenomenon but also highlights its significance in the context of the studied scenario.

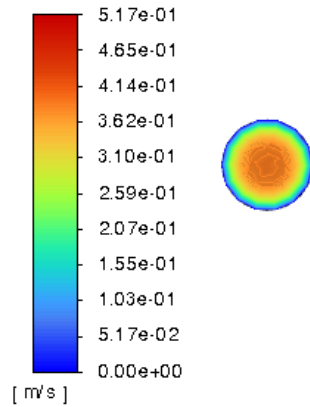


Fig. 4. Contours of velocity at volume fraction of 3%.

For the purpose of assessing and quantifying this heat transfer enhancement, a comparative analysis is conducted by examining the average heat transfer coefficients at different solid-phase volume fractions: specifically, 3%, 4%, 5%, and 6%. These coefficients are compared against the performance of pure water under identical conditions, including heat flux and Reynolds number. The results of this comparative evaluation are visually presented in Fig. 5.

The findings from this comparison are noteworthy. It is evident that, at volume fractions of 3%, 4%, 5%, and 6%, the average heat transfer coefficients for alumina-water nanofluids exhibit substantial enhancements of 9.35%, 14.48%, 19.1%, and 23.5%, respectively, in comparison to pure water. These enhancements underscore the considerable potential of alumina-water nanofluids for significantly improving heat transfer efficiency across a spectrum of applications. Understanding and quantifying such enhancements are vital in engineering design and optimization, as they offer valuable insights into the superior heat transfer capabilities of nanofluids, particularly as a function of solid-phase concentration. These insights inform the development of more efficient and effective heat exchange systems, contributing to advancements in areas such as thermal management, energy conversion, and heat exchanger design.

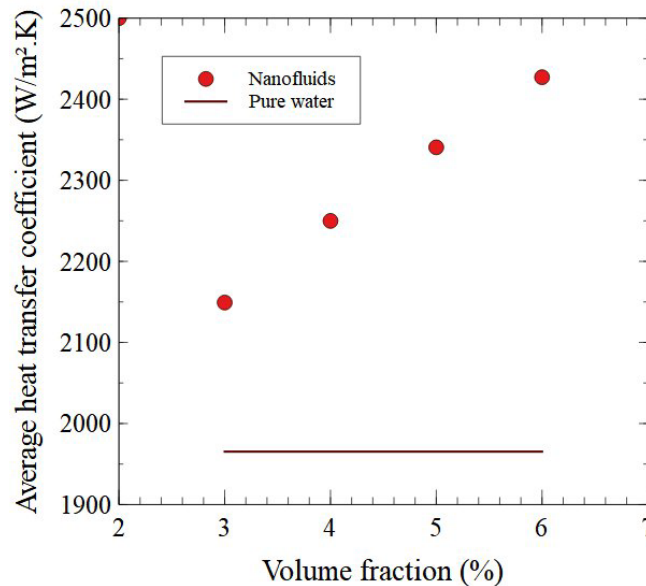


Fig. 5. Comparison of average heat transfer coefficient of water with nanofluids having volume fraction of 3%, 4%, 5%, and 6%.

The study delves into the influence of heat flux on the profile of the local heat transfer coefficient within the system. The findings reveal a notable trend: as the heat flux increases, there is a corresponding rise in the local heat transfer coefficient. This relationship underscores a fundamental principle in heat transfer, where a greater heat input results in enhanced heat transfer rates. To provide a quantitative perspective, the average heat transfer coefficients under various heat flux conditions are computed. The study identifies average heat transfer coefficient values of 1556.345 W/m²·K, 1898.49 W/m²·K, 2149.2 W/m²·K, and 2344.591 W/m²·K for heat flux levels of 50 kW/m², 75 kW/m², 100 kW/m², and 125 kW/m², respectively.

These findings underscore the direct correlation between heat flux and heat transfer coefficients, reaffirming the fundamental principle that higher heat input leads to increased heat transfer rates, as shown in Fig. 6. This knowledge is pivotal in the design and optimization of heat transfer systems across various industries, offering insights into how varying heat flux conditions can be harnessed to achieve specific thermal performance objectives.

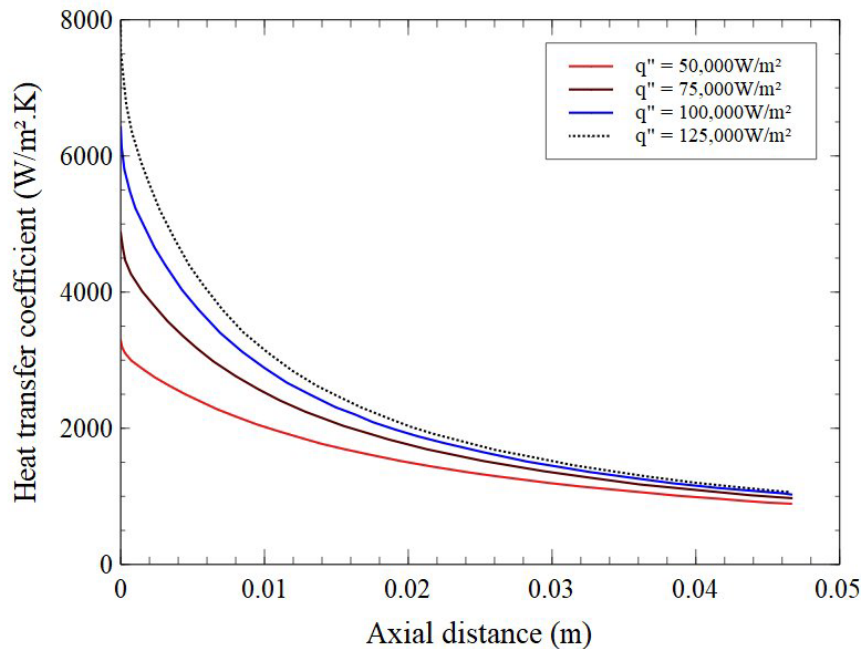


Fig. 6. Comparison of local heat transfer profiles of Al₂O₃-water nanofluids at heat flux of 50 kW/m², 75 kW/m², 100 kW/m², and 125 kW/m².

5. Submitting the Paper

Using a Multiphase Eulerian model, Al₂O₃-water nanofluids with volume fractions ranging from 3% to 6% were simulated, revealing several key findings. First, the Knudsen number decreases with increasing volume fraction and reaches 0.0099 at 2.5%, indicating the validity of continuum assumptions at 2.5% and above. Second, heat transfer improves as the solid phase volume fraction increases within the studied range. Third, a comparison of average heat transfer coefficients between pure water and Al₂O₃-water nanofluids showed enhancements of 9.35%, 14.48%, 19.1%, and 23.5% at volume fractions of 3%, 4%, 5%, and 6%, respectively.

Acknowledgements

Our sincere gratitude extends to ASPIRE for their generous funding (AARE20-358).

References

- [1] A. S. Habeeb, A. A. Karamallah, and S. Aljabair, "Review of computational multi-phase approaches of nano-fluids filled systems," *Therm. Sci. Eng. Prog.*, vol. 28, no. December 2021, p. 101175, 2022, doi: 10.1016/j.tsep.2021.101175.

- [2] M. Mahdavi, M. Sharifpur, and J. P. Meyer, “CFD modelling of heat transfer and pressure drops for nanofluids through vertical tubes in laminar flow by Lagrangian and Eulerian approaches,” *Int. J. Heat Mass Transf.*, vol. 88, pp. 803–813, 2015, doi: 10.1016/j.ijheatmasstransfer.2015.04.112.
- [3] S. Göktepe, K. Atalik, and H. Ertürk, “Comparison of single and two-phase models for nanofluid convection at the entrance of a uniformly heated tube,” *Int. J. Therm. Sci.*, vol. 80, no. 1, pp. 83–92, 2014, doi: 10.1016/j.ijthermalsci.2014.01.014.
- [4] T. Ambreen, A. Saleem, and C. W. Park, “Homogeneous and multiphase analysis of nanofluids containing nonspherical mwcnt and gnp nanoparticles considering the influence of interfacial layering,” *Nanomaterials*, vol. 11, no. 2, pp. 1–22, 2021, doi: 10.3390/nano11020277.
- [5] L. Verma, R. Meher, Z. Hammouch, and H. M. Baskonus, “Effect of heat transfer on hybrid nanofluid flow in converging/diverging channel using fuzzy volume fraction,” *Sci. Rep.*, vol. 12, no. 1, pp. 1–21, 2022, doi: 10.1038/s41598-022-24259-6.
- [6] M. Lucas, P. Kosinski, and B. V. Balakin, “Eulerian-Eulerian model for photothermal energy conversion in nanofluids,” *AIP Conf. Proc.*, vol. 2116, no. September 2011, 2019, doi: 10.1063/1.5113995.
- [7] A. El Jery, S. P. H. Mahmood Salman, S. majeed saeed, and K. Mohamed Khedher, “Comparison of different approaches for numerical modeling of nanofluid subcooled flow boiling and proposing predictive models using artificial neural network,” *Prog. Nucl. Energy*, vol. 156, no. December 2022, p. 104540, 2023, doi: 10.1016/j.pnucene.2022.104540.
- [8] M. Kalteh, A. Abbassi, M. Saffar-Avval, and J. Harting, “Eulerian-Eulerian two-phase numerical simulation of nanofluid laminar forced convection in a microchannel,” *Int. J. Heat Fluid Flow*, vol. 32, no. 1, pp. 107–116, 2011, doi: 10.1016/j.ijheatfluidflow.2010.08.001.
- [9] L. Sirovich, 2005_Karniadakis_Microflows and Nanoflows Fundamentals and Simulation_Springer, vol. 29.
- [10] O. S. Alharbi and A. A. Abdullah, “A revised model for the effect of nanoparticle mass flux on the thermal instability of a nanofluid layer,” *Demonstr. Math.*, vol. 54, no. 1, pp. 488–499, 2021, doi: 10.1515/dema-2021-0045.
- [11] S. Vafaei, J. A. Yeager, P. Daluga, and B. Scherer, “Forced convection nanofluid heat transfer as a function of distance in microchannels,” *Materials (Basel)*, vol. 14, no. 11, 2021, doi: 10.3390/ma14113021.